Nature-based strategies and mechanisms that mitigate coastal floods and minimize induced flooding

P. M. Orton[a*], S. L. Dykstra[b], S.A.Talke[c]

[a] Davidson Laboratory, Department of Civil, Environmental and Ocean Engineering, Stevens Institute of Technology, Castle Point on Hudson, Hoboken, NJ 07030, USA, porton@stevens.edu.
[b] College of Fisheries and Ocean Science, University of Alaska Fairbanks, Fairbanks, AK, USA
[c] Department of Civil & Environmental Engineering, California State Polytechnic University at San Luis Obispo, San Luis Obispo, CA, USA
* corresponding author

Abstract

A challenge with flood mitigation is that the water kept out of one floodplain can be redistributed to other locations. To date, however, the mechanisms and dynamics of coastal flood attenuation and induced flooding are under-researched. In this study, we analyse a 100-year coastal flood for Jamaica Bay, New York, an urbanized bay characterized by near standing-wave tides that provides a relatively simple case study of flood mitigation dynamics. We apply hydrodynamic modelling for detailed quantification of the effects of flood mitigation and idealized 1D semi-analytical modelling to investigate flood wave reflection processes. We evaluate three mitigation scenarios relative to a Control run, including floodplain and marsh restoration (nature-based solution NBS1), inlet narrowing and bay shallowing (NBS2), and a proposed surge barrier/levee system. Results show that the surge barrier system prevents all bay flooding but induces flood wave reflection and amplification outside the protected area. Three mechanisms enable NBS to reduce flooding while minimizing amplification and induced flooding: Flood wave dissipation, storage increases, and partial reflection. The 7.1% of additional bay area (storage) created with NBS1 leads to only a 1.4% reduction in flood wave amplitude in part due to a counteracting 3.1% increase in tidal prism. NBS2 causes a 18% increase in dissipation and a phase-shifted partial reflection that destructively interferes with the interior bay reflected flood wave, minimizing offshore increases in water level and leading to 54 times more flood prevention than initiation. Understanding these physical mechanisms behind NBS can help enable their application through design optimization.

Keywords: Storm surge, tide, flood mitigation, nature-based solutions, storm surge barriers, reflection, New York City

Highlights:

- Coastal flood mitigation is studied with hydrodynamic and idealized semi-analytical modeling
- Mechanisms of flood wave dissipation, storage and reflection are quantified and evaluated
- A storm surge barrier for Jamaica Bay, New York, stops but reflects a 100-year flood wave
- Nature-based strategies can attenuate a storm surge with minimal induced flooding
- Partial reflection shifts the reflected storm surge wave phase, limiting water level increases

1.0 Introduction

A challenge with estuarine and riverine flood mitigation is that preventing a flood in one location may induce flooding in other parts of the system. For example, storm-driven water levels offshore of seawalls and storm surge barriers can rise higher than they would without barriers and, in some cases, cause “induced flooding” (Figueroa & Son, 2024; Kidd et al., 2017; USACE, 2022). Similarly, constructing dykes may prevent local flooding with sea-level rise, but can lead to larger tides and worsened flood risk outside the protected area (e.g., Holleman & Stacey, 2014; Lee et al., 2017). In the United States, coastal storm risk management studies therefore quantify both flood reduction and inducement, and in some cases must develop “Induced Flooding Mitigation Features” outside of barrier-protected areas to address this problem (e.g., USACE, 2022, 2025).

Green and gray infrastructure approaches (such as marshes or storm surge barriers) have been extensively studied for their ability to attenuate extreme storm tides (Murty, 1984; Slinger, 2021). However, there has been relatively limited generalized assessment of the dynamical processes behind reflection and induced flooding. Nederhoff et al. (2025) evaluated the local and remote effects of flood mitigation approaches for 10-year and (nominal) 100-year storm tides, contrasting neighborhood-fronting sea walls and subregional tide gates against floodplain restoration (and their combined effects) for San Francisco Bay. They also studied the effects of relative sea level rise on tides, including influences on tidal energy flux, amplitude and phase. However, the research did not quantify the influence of the mitigation approaches on broader storm surge long wave dynamics.

The influence of construction measures and natural morphological changes on long-wave dynamics (including storm surge and tides) can be usefully interpreted through consideration of the disparate effects of partial and full wave reflections. A partial reflection occurs anytime the phase speed of a wave changes (e.g., Lighthill & Lighthill, 2001); thus, idealized tide models (e.g., Dronkers, 1964; Jay, 1991) suggest that changes in depth, drag coefficient, tidal velocity, and width can all shift the amplitude and phase of the reflected wave (see also Battjes & Labuer, 2014). At a barrier, the wave reflects with a zero-degree phase shift and the same amplitude as the incoming wave, to enforce a zero-flow boundary condition (e.g., Chernetsky et al., 2010). An example of a naturally occurring partial reflection is the Tongue Point headland in the Columbia River Estuary, which reduces energy flux upstream and causes a tidal amplification downstream (Giese & Jay, 1989). Dredging, channel modification, and changed river flow routing has likely altered this partial reflection and influenced the long-term evolution of tides downstream (Helaire et al., 2019; Talke et al., 2020). Using both idealized modeling and in-situ data, Dykstra et al. (2024) investigated the locations in a convergent estuary where partial and full reflections dominated tidal and storm surge dynamics. They showed that near the barrier, the full reflected wave dominates, with a zone of influence downstream that grows larger as the wave period increases. Partial reflections caused by the narrowing of the estuary in the upstream direction (i.e., convergence) are more important at locations further away from the dam. Most natural or anthropogenically influenced coastal-plain and drowned river valley estuary systems exhibit large geometric variations in depth and width within tidal marshes and complex fractal, convergent channels (Wright et al., 1973). Given that geometric variations in depth and width are ubiquitous features of estuaries, partial reflection dynamics are likely more important than commonly understood.

It is well-established that large expanses of tidal marshes can reduce storm surge or tidal flooding by increasing frictional dissipation and expanding estuary surface area (e.g., Brand et al., 2025; Holleman & Stacey, 2014; Wamsley et al., 2010). However, the improved understanding of reflection processes noted above raises questions about whether our scientific understanding of nature-based solutions could benefit from deeper mechanistic and dynamical analyses. Tidal marshes are often cited for their ability to "dissipate" storm surge (Rezaie et al., 2020), yet little if any research has directly quantified their influence on energy dissipation for estuary-scale mitigation of long waves. For example, while Sheng et al. (2012) computed a Vegetation Dissipation Potential for storm surge, it was computed only from the modeled flood water volume with and without vegetation. Yet, marshes constitute abrupt changes in friction and are often sites of hydrodynamic convergence, so partial reflections may play a role in their flood attenuation benefits.

The present research addresses this research gap by focusing on the mechanics and dynamics of coastal flood mitigation and inducement, highlighting the differences between nature-based and gray infrastructure mitigation strategies. We study Jamaica Bay as a relatively simple back-barrier estuary system due to its small size (72 km^2), lack of significant streamflow and stratification, deep dredged inlet and channels, and nearly standing wave tides (Pareja-Roman et al., 2023). The primary questions we address are:

- Which nature-based or gray-infrastructure approach reduces water level and flood area most effectively for this system, and why?
- How, where, and why is flooding induced elsewhere for different types of green and gray infrastructure?
- How do the differing dynamical responses caused by partial and full reflections, along with energy dissipation, help explain differences in outcomes between the tested scenarios?

To address these questions, we use hydrodynamic modelling and idealized, semi-analytical modelling of three possible Jamaica Bay flood mitigation scenarios for 100-year coastal flood events to quantify flood reductions and induced flooding. The three scenarios are based on previously proposed flood mitigation approaches for the Bay and include: (a) closure of the bay's inlet with a surge barrier; (b) perimeter and wetland/floodplain restoration, creating an increase in bay surface area; and (c) inlet narrowing combined with channel shallowing.

2.0 Methods

In this section, we introduce the study site (**Section 2.1**), hydrodynamic model and domain (**2.2**), storm selection and meteorological forcing (**2.3**), gray and NBS flood mitigation scenarios (**2.4**) and a set of dynamically relevant computations for dissipation, storage, inlet choking and wave reflection and partial reflection (**2.5**). The idealized, semi-analytical modeling approach is introduced (**2.6**), building upon the prior methods and describing our method for quantifying the amplitudes and phases of reflected long waves. Lastly, we acknowledge limitations of our study's approach in **Section 2.7**.

2.1 Location

Jamaica Bay is a mesotidal, heavily urbanized lagoonal estuary at the south-eastern edge of New York City. The semidiurnal tide is predominantly a reflected, standing wave with a range from 1.5-3.5 m (Chant et al., 2021). The bay's waters are typically weakly stratified or well mixed due to small average freshwater inputs of ~10 m^3/s ; thus, the typical tidal discharge is approximately 700 times larger than the average freshwater discharge (Pareja-Roman et al., 2023). The bay's "urbanized" geometry arises from major historical anthropogenic alterations in the 20th century, which changed Jamaica Bay from a tidally damped, shallow, lagoonal system with a small number of narrow, deep channels, to a port and bay region with amplified tides. The average water depth of the bay-inlet system increased from 1.7 to 4.5 m, tidal surface area decreased from 92 to 72 km^2, and the inlet minimum cross-sectional area expanded from 4800 to 8900 m^2. As a result of these modifications, the 100-year storm tide has increased by 12% in the bay since the 1800s (Orton et al., 2020) and the mean tidal range has increased by 20%. Due to a combination of amplified tides and relative sea-level rise, the bay margins are now subject to chronic flooding (over 20 minor floods per year at some locations; Pareja-Roman et al., 2023). Tidal amplification is driven by reduced tidal energy dissipation at the bay's inlet and increased tide wave reflection in the bay interior (Pareja-Roman et al., 2023). This improving understanding of the negative effects of anthropogenic historical alterations on flood risk motivates exploration of nature-based flood mitigation solutions which mimic the historical landscape (e.g., Fischbach et al., 2018; Orton, MacManus, et al., 2016; Orton et al., 2015; Seavitt et al., 2015).

2.2. Hydrodynamic modelling

Water levels are simulated using the Stevens Estuarine and Coastal Ocean Model's vertically integrated mode, sECOM-2D (Blumberg et al., 1999) with wetting and drying (Blumberg et al., 2015). The Jamaica Bay model is based on a 1,069×550 structured grid with a resolution of 30 m (Orton et al., 2015). Bottom friction is simulated using Manning's n values that are based on landscape type (e.g., salt marsh, estuary open water), using categories from the National Land-Cover Database (NLCD) (e.g., Mattocks & Forbes, 2008). The Jamaica Bay model grid is one-way nested inside the regional New York Harbor Observing and Prediction System (NYHOPS) grid, which is likewise nested inside the Stevens Northwest Atlantic Predictions grid (Orton et al., 2020). A radiating water level boundary condition is used to transfer water levels from NYHOPS to the Jamaica Bay domain (Reid & Bodine, 1968). The Jamaica Bay model's water level predictions have been evaluated with a root mean square error (RMSE) of 0.07 m for a year-long simulation (Pareja-Roman et al., 2023) and 0.19 m for peak water levels and high-water marks for Hurricane Sandy (Orton et al., 2015).

2.3 Storm selection and meteorological forcing

Effects of different flood mitigation strategies are investigated using simulations of 22 tropical cyclone (TC) driven, 100-year storm tide events. These events were selected from a New York City (NYC) probabilistic flood hazard assessment (Orton, Hall, et al., 2016) that was downscaled to Jamaica Bay (Orton et al., 2020). The NYC flood hazard assessment found that 100-year storm tide events nearby at The Battery (peaking at 2.8 m NAVD88, for a 2025 local mean sea level) were almost exclusively caused by TCs. The NYC assessment included 1516 storm simulations (606 synthetic TCs and 961 extratropical cyclones) and determined present-day return levels for 10-year to 10000-year return periods (Orton, Hall, et al., 2016). The synthetic TCs were created based on a validated statistical-stochastic model of a million years of present-day North Atlantic TCs (Hall & Yonekura, 2013), with wind and pressure fields based on parametric models (Orton, Hall, et al., 2016). The NYHOPS domain results for The Battery using these synthetic TC forcings were found to have an RMSE on peak storm tide values of 0.32 m for 12 historical TCs (Orton, Hall, et al., 2016).

The remainder of the paper focuses on a comprehensive analysis of a single storm tide event that exhibits strong reflection in simulations with a storm surge barrier across Jamaica Bay's inlet. This event is caused by a category-3 hurricane for which storm surge peaks soon after the time of expected high tide (**Figure 1**) causing a peak rise rate of 0.93 m h^{-1} (the 2^{nd} highest of 22). The

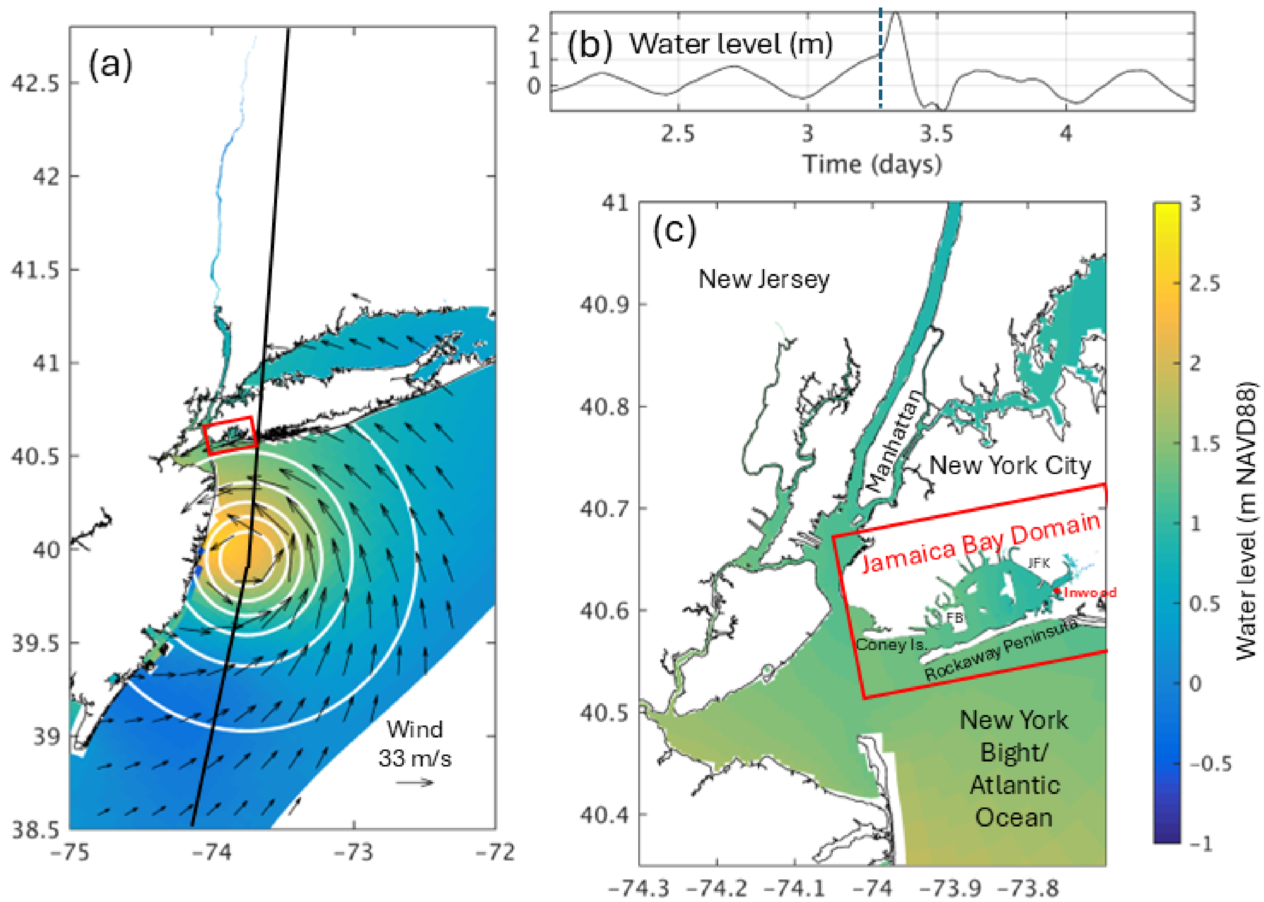

Figure 1: The primary Category-3 hurricane and storm tide simulation utilized in this study. (a) The northward-directed storm track (black line), pressure isobars (white lines) and wind velocity (black vectors). (b) Time series of water level at the southern tip of Manhattan (The Battery) with the time of the shade plots marked with the dashed line. (c) Storm tide (water elevation) shading in a zoom-in map view of New York/New Jersey Harbor and Jamaica Bay sub-domain (red rectangle). Locations marked include Inwood (tide gauge marked, in red), Coney Island (Coney Is.), John F. Kennedy Airport (JFK) and Floyd Bennett Field (FB) by the narrowest part of the inlet.

combined tide and storm surge cause an increase in peak water level of 1.0 m just offshore of the barrier (relative to the no-barrier case). This induced increase in water level is the largest of the 22 events but not exceptional; three other events exhibit increases exceeding 0.6 m. Small or negligible increases below 0.1 m are found for 14 events. Results of the broader set of 22 simulations (Supplementary Materials Section SM1) show that events with faster water rise rates have the most propensity for a larger increase in offshore water level (a linear correlation coefficient of 0.74; Figure SM1).

2.4 Flood mitigation scenarios

A control model and three experimentally modified model scenarios are applied in simulations of the TC (**Figure 2**). The Control scenario/DEM is discussed in **Section 2.2**. The Rockaway Inlet storm surge barriers and levees scenario approximates the Tentatively Selected Plan (TSP) from the NY/NJ Harbor and Tributaries Study (USACE, 2022). It includes a large, gated surge barrier crossing Rockaway Inlet at Floyd Bennett Field (FB in **Figure 1**), two smaller gated surge barriers at inlets to a bay (Sheepshead) and creek (Gerritsen) just west of FB, and a series of levees along the external coastline (**Figure 2**). Two additional, nature-based solution (NBS) scenarios are based on interventions suggested in prior studies and were co-generated in workshops with stakeholders (Fischbach et al., 2018; Orton, MacManus, et al., 2016). Changes to inlet and bay geometry are described below and summarized in **Table 1**.

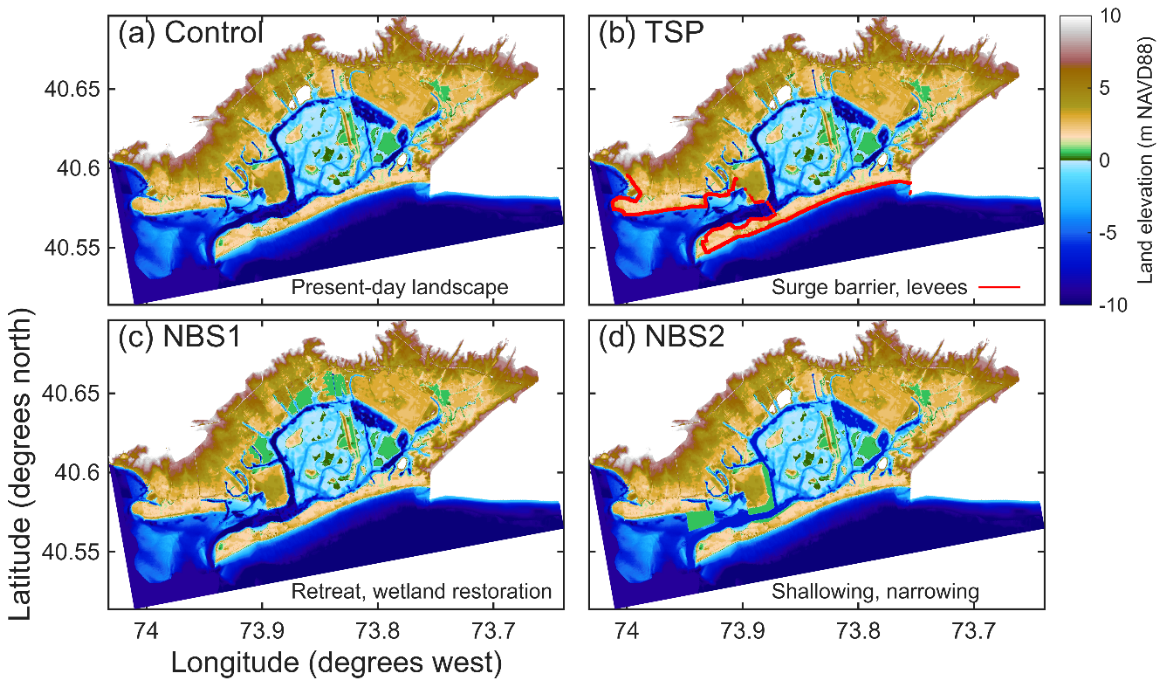

Figure 2: Digital elevation models for (a) Control, (b) tentatively selected plan (TSP), and nature-based solutions (c) NBS1 and (d) NBS2.

The NBS1 retreat and wetland restoration scenario is implemented in the model by converting low-lying (<2.5 m elevation) interior bay neighborhoods and a (park-covered) garbage dump to wetlands. Open land after retreat is excavated to an elevation of 0.5 m (relative to mean sea level), a typical elevation for healthy present-day marshes in the Bay (Fischbach et al. 2018). The roughness typical of marshes is simulated by increasing the Mannings-n to 0.045 s $m^{-1/3}$ (Mattocks & Forbes, 2008), raised from a default value of 0.02 (Pareja-Roman et al., 2023). This flood mitigation strategy arose from attendees in a workshop (Orton, MacManus, et al., 2016) where historical maps of natural marshes and floodplains were shown to attendees (Orton et al., 2020). It was of interest because it was an opportunity for marsh restoration and because it involves neighborhoods that already have chronic high-tide flooding (Pareja-Roman et al., 2023; Patrick et al., 2019). Prior studies of Jamaica Bay determined that the restoration of interior marsh islands at the center of the bay yielded little damping of storm tides and reduction in flood hazards. Effectively, waters continued to move unobstructed through the deep channels along the perimeter of the bay (Marsooli et al., 2016; Orton et al., 2015).

The NBS2 inlet narrowing and bay/inlet shallowing scenario, initially called "channel repair" (Orton, MacManus, et al., 2016), was developed based on evidence that the historical bay system damped tides and storm surges due to its smaller inlet cross-section and shallower, more dissipative tidal channels (Orton et al., 2015). The NBS2 scenario includes relatively substantial geometric changes; the average inlet width at Floyd Bennett Field (**Figure 1**) is reduced from 1100 to 500 m and the inlet depth at that location is reduced from 8.5 to 6.8 m. An additional less extreme inlet width reduction is added at the western end of the inlet, at the end of Rockaway Peninsula (**Figure 2d**). Bay channels are reduced from 8-12 m to 6.8 m below NAVD88. Resulting averages for bay and inlet geometric parameters are shown in **Table 1**. While pre-development interior bay channels were far shallower (Orton et al., 2020), the shallowing here is capped at 6.8 m NAVD88, the federally authorized shipping channel depth required for local shipping (Orton, MacManus, et al., 2016). The model for the NBS2 scenario includes a slight bed roughening to a Manning's n value of 0.025, on the assumption that natural bedforms would form due to stronger near-bed currents (an increase in bed roughness could also be engineered). Previous model experiments showed that this roughening leads to only a modest additional flood reduction (Orton, MacManus, et al., 2016). The concept of imposing shallowing and narrowing on an underutilized port like Jamaica Bay remains exploratory and additional study concerning water quality, design, engineering and morphodynamic evolution would be required before implementation.

Table 1: Bay and inlet geometry and friction parameters for control and adaptation scenarios

	Inlet width average	**Inlet depth average**	**Interior bay depth average**	**Inlet length**	**Channel Mannings number**	**Marsh Mannings number**
	b	**H**	**H_bay**	**L**	**n**	**n**
	(m)	**(m)**	**(m)**	**(m)**	**(s $m^{-1/3}$)**	**(s $m^{-1/3}$)**
Control	1970	6.24	2.9	5940	0.02	0.045
TSP	1970	6.24	2.9	5940	0.02	0.045
NBS1	1970	6.24	2.9	5940	0.02	0.045
NBS2	1380	5.11	2.35	5940	0.025	0.045

2.5 Additional dynamically relevant computations

Local Maximum and Total Dissipation: One way that nature-based solutions reduce water levels is by enhancing the damping and dissipation of shallow water waves, thus altering the velocity, amplitude, and reflection characteristics of shallow-water (long) waves such as storm surge and tides. The depth-integrated dissipation is estimated at each point in the Jamaica Bay model grid using

$$\varepsilon = \rho C_D |U| U^2 , \quad (1)$$

where C_D is the bed drag coefficient, ρ is the density of water, the water velocity is U, and the absolute value makes the quantity positive-definite. This equation leverages the scaling of dissipation as shear production (stress times shear), applies the quadratic drag law for stress, and is vertically integrated over the water column (Taylor, 1920; Gill, 1982). The drag coefficient is computed from the Mannings-*n* coefficient using the standard formula, $C_D = g\, n^2\, h^{-1/3}$, where g is gravity and h is water depth. The temporal maximum dissipation rate (in W m^{-2}) is computed as the local maximum on every wetted grid cell during the rising storm tide. The bay-wide (inlet included) total dissipation during the rising arm of the storm-tide hydrograph is computed as the integral of dissipation over the area of the bay (and floodplain), evaluated over the period of the rising storm tide. This dissipation value represents the energy loss of the incoming wave.

For a simple scale comparison to total dissipation, the change in total energy within Jamaica Bay is approximated as the change in potential energy between low tide and the peak water level, integrated over the bay area (see Supplementary Material **Section SM2**). This computation assumes that peak water levels within the Bay occur at the same time, with a negligible phase shift, a reasonable approximation in a standing wave system.

Box model and two simplified water level change estimates: A flood wave's height can potentially be reduced by increasing bay surface area, thus spreading the wave horizontally. For a given flow volume P_R (i.e., prism) spread over an area A_e, mass balance suggests that the flood wave height (total increase in water level) is $h = \frac{P_R}{A_e,}$ neglecting hypsometric effects in intertidal areas and freshwater inflow (assumed small here). An increase in area A_e will reduce h, but only if the prism of water entering the bay doesn't proportionally increase. The relative effects of area and prism change can be assessed by differentiating *h* with respect to A_e, which yields the following (expressed in difference form)

$$\frac{\Delta h}{\Delta A_e} = \frac{1}{A_e,}\frac{\Delta P_R}{\Delta A_e} - \frac{P_R}{{A_e}^2} \quad (2)$$

Or

$$\Delta h = h\left(\frac{\Delta P_R}{P_R} - \frac{\Delta A_e}{A_e}\right) \quad (3)$$

Effectively, the fractional change in flood wave height, $\Delta h/h$, is related to the fractional change in area ($\frac{\Delta A_e}{A_e}$); however, this decrease is counteracted by any fractional increase in the prism $\frac{\Delta P_R}{P_R}$ caused by a tide or storm tide. This simplified expression assumes an approximately standing wave behavior, as previously observed for Jamaica Bay (e..g, Pareja-Roman et al., 2023) and is inappropriate to apply in larger basins with a significant phase progression. Here, we determine the efficacy of fractional increases in area by also evaluating the modeled change in storm-tide prism, using simulation results. Two simple scale estimates for water level reduction are thus available for testing for our study; In the first, neglecting the first term on the right side of Equation 3, one makes a simple scale estimate that a percent increase in bay area leads to a proportional percent reduction in flood wave height, which requires no modelling; in the second, the one applies the full box model computation of Equation 3, which requires our 2D modeling results to estimate prism change.

Choking Number: A nondimensional parameter that provides some dynamical understanding of long wave (tide or storm surge) transmission into a back-barrier (or similarly, lagoonal) estuary is the Choking Number (Keulegan, 1967; Stigebrandt, 1980):

$$P = \left(\frac{gb^2H^3T^2}{C_d L \eta_o A_e^2}\right)^{1/2} \quad (4)$$

Here, g is gravitational acceleration, b is inlet width, H is inlet depth, T is wave period, C_D is bottom drag coefficient, L is inlet length, and η_o is the offshore wave amplitude. The Choking Number was derived from a 1D linearized momentum balance and conservation of mass in an idealized bay-inlet system. It has been suggested that values P<<5 represent strong damping of the offshore wave, and values P>10 represent little or no damping (MacMahan et al., 2014; Stigebrandt, 1980). Choking computations for Control and NBS1 utilize the Control b, H and L (1970, 6.24 and 5940 m, respectively; **Table 1**), while that for NBS2 use the adjusted mean H of 5.11 m and b of 1380 m. No computation is made for the closed off TSP surge barrier plan due to its complete closure of the inlet. T is estimated as 6 h (combining surge and semidiurnal tide periods; **Figure 1b**) and A_e estimates for Control, NBS1 and NBS2 are all based on the model results during the event.

Wave Reflection: Wave propagation in estuaries is influenced by both full and partial reflections (e.g., Battjes & Labuer, 2014; Dronkers, 1964; Dykstra et al., 2024; Eagleson & Dean, 1966; Ippen, 1962; Jay, 1991; Spicer et al., 2024; Talke et al., 2021). In a full tidal reflection, a zero-flow boundary condition is applied and a zero-degree phase shift results; the peak in the reflected wave moves in the opposite direction of the incoming wave, causing constructive interference. A partial reflection occurs anytime that the phase speed of a (shallow-water) wave changes (e.g., Georgas, 2012; Lighthill & Lighthill, 2001). The equation of a tide wave in a prismatic channel with no river flow can be represented as:

$$\eta(x,t) = \underbrace{A(x)\cos(\omega t + k_f x)}_{Reflected\ Wave} + \underbrace{B(x)\cos(\omega t - k_f x)}_{Incident\ Wave} = Re\left[\left(\underbrace{A(x)e^{k_f x}}_{Reflected\ Wave} + \underbrace{B(x)e^{-k_f x}}_{Incident\ Wave}\right)e^{i\omega t}\right] \quad (5)$$

where x is a spatial coordinate that begins at the coast and increases landward, $\omega = \frac{2\pi}{T}$ is angular frequency, A and B are amplitudes, and Re denotes the real term. The wavenumber $k = \frac{2\pi}{\lambda}$ (λ is wavelength) deviates from the inviscid dispersion relation ($k = \frac{\omega}{\sqrt{gH}}$) , as it is modified by friction:

$$k_f = \frac{\omega}{\sqrt{gH}}\sqrt{-1 + i\frac{r}{\omega}}, \quad (6)$$

where frictional effects are linearized as:

$$r = \frac{8}{3\pi}\frac{C_d U}{H}, \quad (7)$$

and *U* is peak water speed and *H* is depth. These equations show that frictional effects scale with water speed (Eq. 7) and act to increase the wavenumber (Eq. 6). Thus, frictional effects slow the wave speed $c = \frac{k_f}{\omega}$, for both the incident and reflected waves, in addition to causing amplitude attenuation. Any change to velocity, drag coefficient, or depth potentially alters the complex wave number. Similarly, changes in the dominant frequency of the incident long wave (either storm surge or tide) will influence the solution (e.g., Familkhalili et al., 2020). A process that increases wave celerity or a reduction in cross-sectional area generates a positive reflected wave where wave interference is positive and when a wave slows or the cross-sectional area increases a negative reflected wave is generated where the interference is negative (Battjes & Labuer, 2014; Ippen, 1962). The phase of the reflected wave is a combination of any full reflection or partial reflection from elsewhere in the domain (e.g., Dykstra et al., 2024). It must fulfill the mass and momentum balance constraints but is not constrained to be zero degrees (a similar phenomenon is observed in the transmission of electricity along power lines; Murty, 1984). Thus, it is possible for a partial reflection to be induced that does not add to, and possibly destructively interferes with, the incoming wave.

2.6 Idealized 1D semi-analytical modeling

In this study, we evaluate long-wave dynamics and partial reflections using a simplified 1D semi-analytical model, developed by Talke (2021) and based on Dronkers (1964). The 1D model uses linearized friction (Eq. 7) and is applied on an idealized geometry that is similar to the bathymetry of Jamaica Bay (see below). Analytical wave equations are based on Dronkers (1964) and Jay (1991) and separate a total wave amplitude η into contributions from the incident and reflected wave components (Eq. 5). The modelling solution divides the domain into multiple segments (here, of 100 m length), which enables the influence of spatially variable velocity *U* to be incorporated into frictional effects (Eq. 7). Thus, the influence of *U*(x) on the wave number (Eq. 6) is assessed, and hence its influence on spatially variable reflection dynamics. A single sinusoidal wave is prescribed at the open boundary, and no-flow is enforced at the upstream boundary. The model solves for *A(x)* and *B(x)* iteratively. Dykstra et al. (2024) used this model to evaluate both tidal and storm-surge dynamics in a convergent river estuary; here, we apply a similar approach to evaluate how long-waves are altered in a lagoonal estuary, as inlet and bay dimensions are altered.

Our idealized geometry (**Figure 3**) resembles a simplified version of the Control, TSP (barrier), NBS1, and NBS2 scenarios that are modeled numerically (**Figure 2**). The Control, NBS1, and NBS2 scenarios consist of an outer basin, a constricted inlet section, and a wider, shallower bay. Depending on the scenario, there is either a larger bay (NBS1), or a width and depth constricted section from km 8-10 (NBS2) at Floyd Bennett Field (FB in **Figure 1**). The TSP scenario is shortened to 10 km, representing a dam. The NBS1 scenario simulates the expanded domain area by extending the Control domain by 1 km to a depth of 2 m. The NBS2 scenario narrows the inlet from 1600 m to 700 m and reduces the depth from 8.4 m to 6.4 m, closely approximating the average changes in the numerical model. However, to align similar dynamics in each simple model geometry, the representation of NBS2 concentrates the narrowing and shallowing into one short section from 8-10 km, whereas the 2D model has shallowing and choking spread over a longer area.

In NBS2, the bay is also shallowed from a mean depth of 2.90 m (Control) to a value of 2.35 m, again matching the values in the numerical model scenarios. Drag coefficients are set to 0.002 (Mannings-n = 0.020) except for the NBS2 scenario with its roughening calling for a value of 0.003 (n = 0.025).

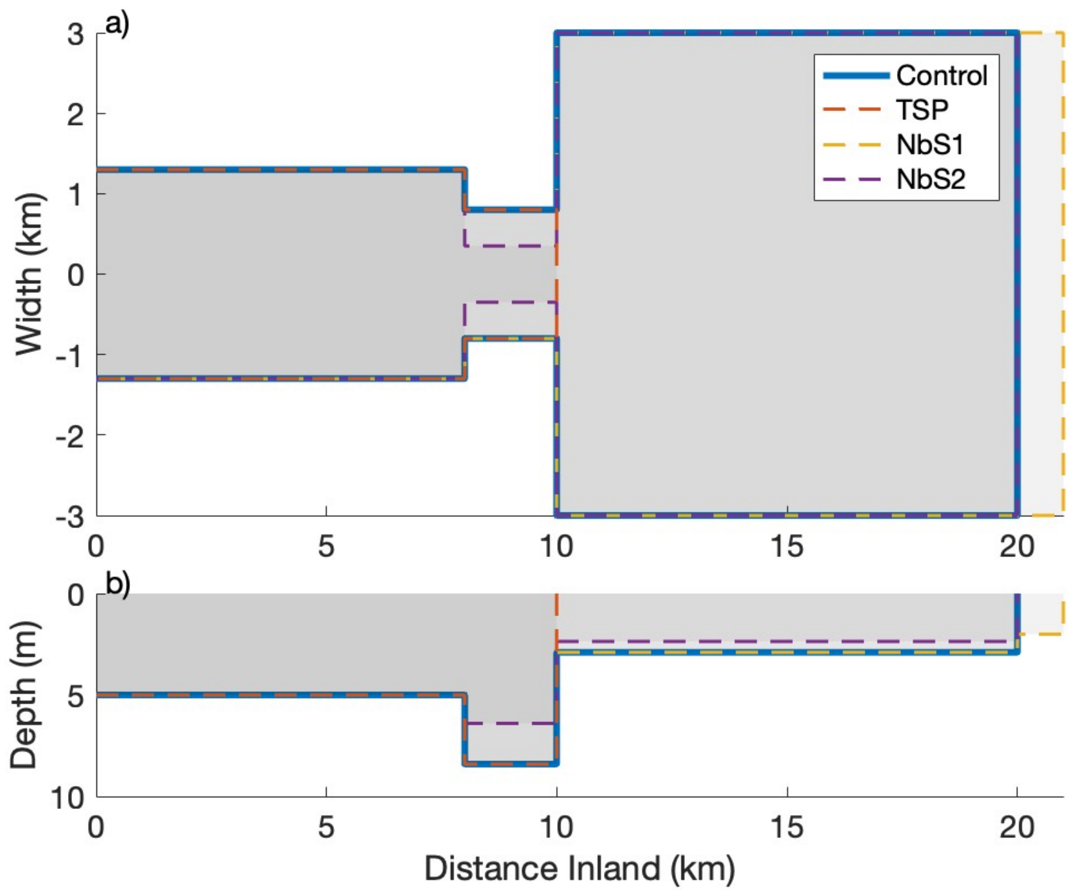

Figure 3: Idealized model domain for the 1D semi-analytical wave model.

2.7 Potential methodological limitations

The numerical simulations on the Jamaica Bay sECOM-2D sub-model are designed to capture the processes relevant to isolate effects of flood mitigation on storm surge and tide and are not intended to capture all dimensions of flood risk reduction. The 2D simulations do not include wind waves, which can be an additional hazard and add to the storm tide through wave runup or overtopping (Hu et al., 2018). The 3D numerical simulations on the regional SNAP/NYHOPS domains include wind waves and their effects on wind drag, bed stress, and water levels (Orton, Hall, et al., 2016), so wave-hydrodynamic coupling in the larger region is accounted for and reflected in the Jamaica Bay model validation. In 2D tide and storm surge modeling studies, a common simplified approach for representing the effects of wetlands is to treat them as enhanced landscape roughness features (Gupta et al., 2025; Szpilka et al., 2016), as was done here. However, more detailed 3D hydrodynamic modeling can be utilized, as well as detailed wave-current-vegetation interaction modeling (e.g., Kalra et al., 2021), and these techniques could give better accuracy than our simplified approach. Lastly, one-way model nesting, even though applying a radiating boundary condition on the Jamaica Bay grid (**Section 2.2**), may introduce boundary effects in our area of interest, particularly offshore of Jamaica Bay's inlet. However, simulations on the regional (NYHOPS) domain that included the adaptation scenarios, though at relatively coarse resolution, were found to replicate the results of the nested simulations, including the reflection and increased water levels outside the bay for the TSP surge barrier scenario.

3.0 Results

Below, we describe the results of the 2D flood modeling of each mitigation scenario, then use these data to quantify flood reductions and induced flooding (**Section 3.1**) and dynamical and energetic characteristics of long-waves and flooding (**Section 3.2**). We end the section with a focused analysis of the properties of reflected and incident long waves (tide, storm surge) based on the 1D semi-analytical modeling (**Section 3.3**). This ordering of information is chosen to begin with detailed modeling results followed by focused process analysis.

Peak water level maps for the Control scenario (**Figure 4a**) show that spatial maximum water levels of about 3.4 m occur south of the Rockaway Peninsula due to strong onshore wind forcing and nearby landfall of the low-pressure center (**Figure 1**). Over the southwestern part of Rockaway Peninsula, a small amount of water is simulated to cross from the ocean to the bay but has little effect on Jamaica Bay water levels. The bayside peak water levels are lower than those at the open coast, potentially due to a choking effect of the existing inlet on the fast-rising storm surge (explored below in **Sections 3.2-3.3**) and east winds resisting the storm surge entry into the bay. Simulated water levels inside the bay peak on the east side at ~2.8 m and on the west side at ~2.4 m (**Figure 4a**). As a result, widespread flooding of neighborhoods alongside the bay interior occurs. Rockaway Peninsula gets flooded from the bay even though water levels are lower there than offshore to the south. This is because the bay side developed land is built on top of landfill over wetlands and has a relatively low elevation (Orton et al., 2020). At the easternmost part of the domain, a roadway berm partially obstructs the flooding and peak water levels are below 1.8 m.

The TSP eliminates all flooding in the bay while not causing induced flooding outside the bay (**Figure 4b**). The TSP system was designed for a USACE estimate of the 100-year coastal flood that is slightly higher than the estimate of Orton et al. (2020), plus an additional 0.6 m of freeboard. Thus, in this case, the increased water level caused by reflection off the seawall/dam does not translate into additional flooding, primarily because the design height of the infrastructure is above the increased water levels. Nonetheless, our results support the prior finding that one must design for long wave reflection and higher offshore water levels with Induced Flooding Mitigation Features (e.g., USACE, 2022).

The NBS1 coastal retreat, excavation and wetland restoration produces only minor reductions in peak water levels within Jamaica Bay, while the shallowing/narrowing (NBS2) scenario significantly reduces peak water levels relative to the Control scenario (**Figure 4c,d**). The NBS1 scenario peak water levels in the bay are similar to Control (2.4-3.0 m) and the NBS2 peak water levels are reduced to 1.7-2.4 m. As a result, overland flooding around the bay is nearly the same in NBS1 as Control, apart from the additional flooded area where retreat and excavation occurred on the northern edge of the bay. Overland flooding is reduced with NBS2 but still widespread across the Rockaway Peninsula, in spite of lowered peak water levels in the bay.

Time series of the water levels at Inwood (**Figure 5**), near the eastern end of the bay, reveal the effects of each adaptation scenario on peak water levels and tides within the bay. Peak water levels at Inwood (and similarly for averages across the bay) are reduced below Control for NBS1 by 4 cm, for NBS2 by 63 cm, and for TSP by well over 2 m. Effects on tides are revealed in the time series prior to the storm event, showing a very slight amplitude reduction by NBS1 and a larger reduction of about 5-10% by NBS2. The TSP scenario inherits the water-level at the time of the barrier closure, in this case the mean sea-level of 0.0 m NAVD88, but winds drive up higher peak localized water levels with a mean of 0.18 m.

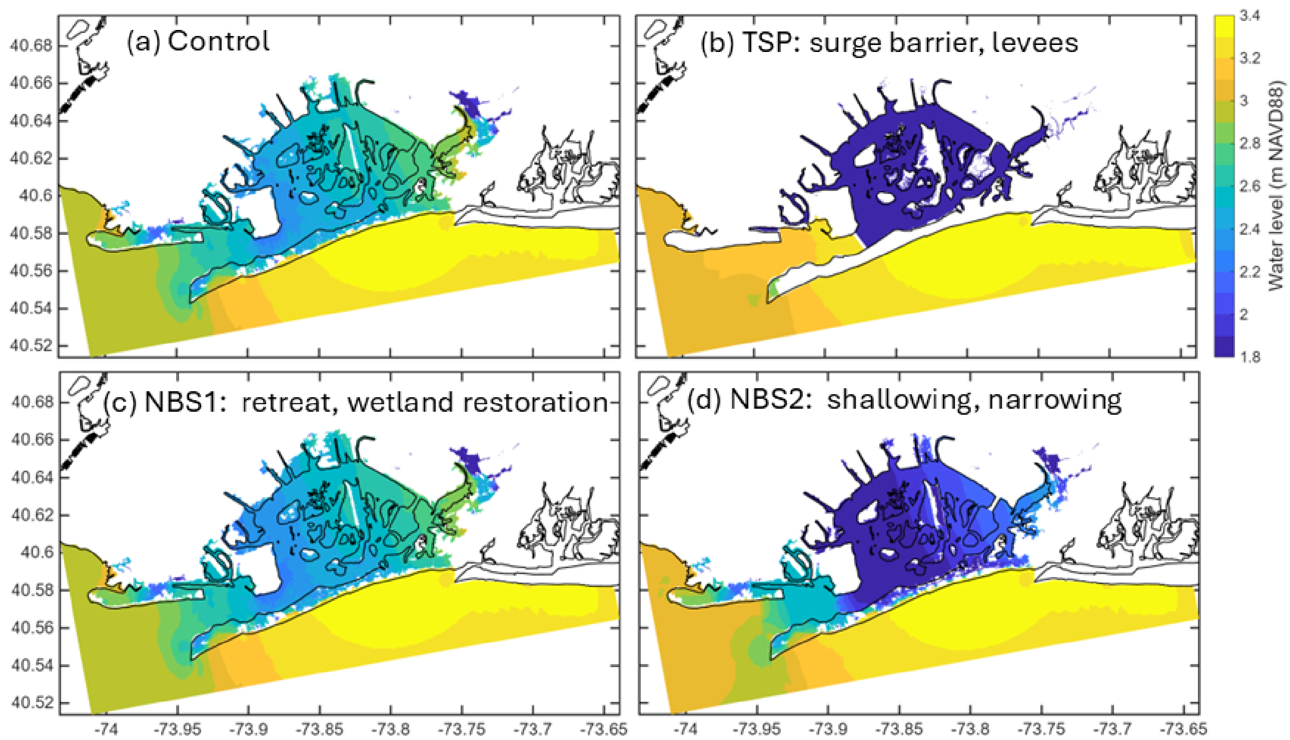

Figure 4: Maps of modeled peak water level results for the 100-year TC event under (a) Control, (b) TSP, (c) NBS1 and (d) NBS2 flood mitigation scenarios. TSP water levels inside the bay are off scale on the color bar, below 1 m.

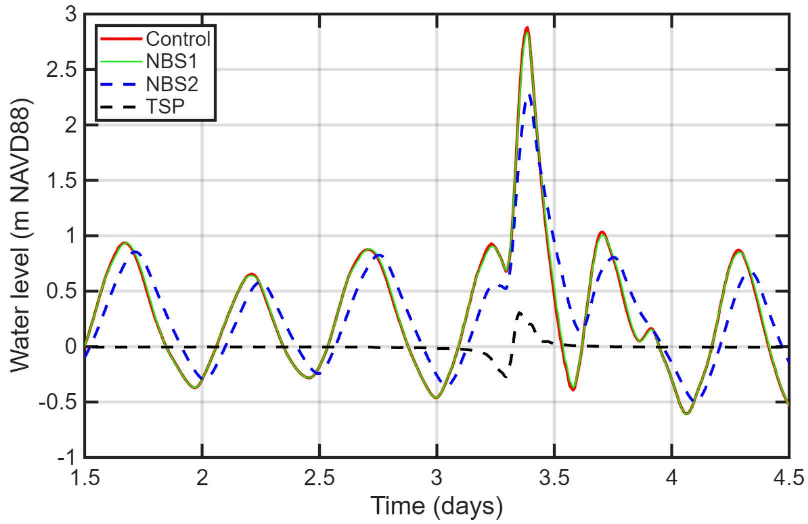

Figure 5: Water level time series for Control and the three mitigation scenarios at Inwood, Jamaica Bay (location shown in **Figure 1**).

3.1 Flood prevention and initiation

Flood changes relative to Control are shaded in **Figure 6** and help reveal increases offshore of the bay. In the TSP simulation, peak water levels are raised by 1.0 m immediately seaward of the barrier, with values declining with distance offshore. The NBS2 scenario shows a smaller increase in this region, peaking at 0.2 m. No increase in inlet water levels is observed in the NBS1 results.

Flooding was prevented to varying degrees by the mitigation scenarios, meaning that it occurred in Control and did not occur in the mitigation scenario (black dots in **Figure 6**). Conversely, some additional flooding was initiated in all scenarios, relative to Control (red dots in **Figure 6**). The total land area in which flooding is prevented varies strongly by mitigation scenario (**Table 2**), with the most reduction under the TSP scenario (40.8 km^2), followed by the NBS2 scenario (9.5 km^2) and the NBS2 scenario (1.4 km^2). For all three mitigation scenarios, the new flood area initiated is relatively small. The small amount of induced flooding under the TSP scenario (0.18 km^2) arises due to surge barrier being supplemented with levees and other protective measures for populated areas outside the bay. The induced flooding occurs in areas such as the uninhabited western tip of Rockaway Peninsula, and the area is 224 times smaller than the area of prevented flooding (41 km^2). Flood area initiated for NBS2 is 0.17 km^2, which is 54 times smaller than the 9.5 km^2 prevented. Flood area initiated for NBS1 excludes the area intentionally flooded and amounts to about 0.07 km^2 of new flooding, a 12 times smaller area than the flood area prevented (0.8 km^2).

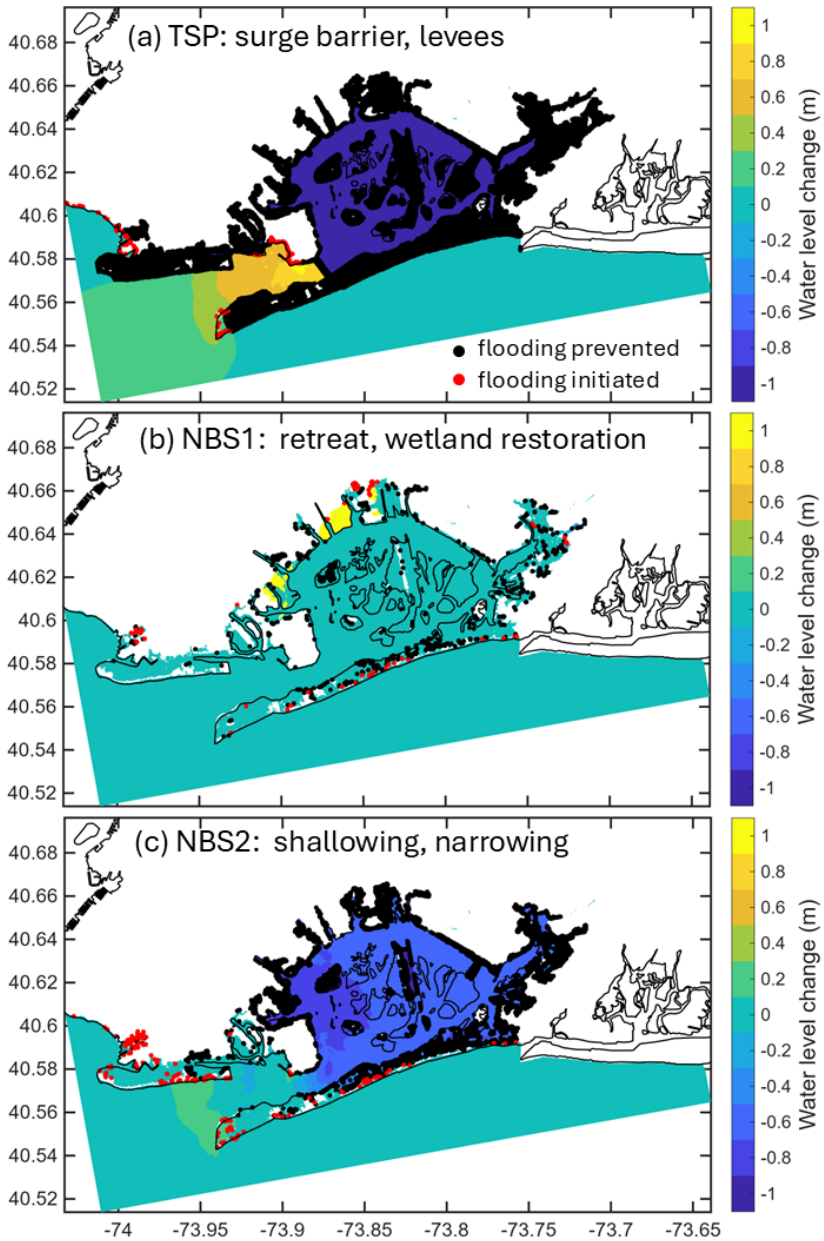

Figure 6: Changes in peak water levels for each mitigation scenario, relative to Control. Red dots show locations in which new flooding was initiated, and black dots show prevented flooding (relative to Control).

Table 2: Land area subject to flood prevention or initiation under three mitigation scenarios

	TSP	NBS1	NBS2
Flood area prevented	41 km^2	0.8 km^2	9.5 km^2
Flood area initiated	[a]0.18 km^2	[b]0.07 km^2	0.17 km^2

[a] Small due to high levees offshore of barrier
[b] Outside of area intentionally flooded

3.2 Dynamics and energetics of long waves and flooding

Flood reductions in our nature-based scenarios are qualitatively consistent with the changes to the inlet choking number P. The choking number (**Table 3**) is affected much more dramatically by NBS2 shallowing/narrowing than by the small bay interior area change of NBS1. The choking number for the Control scenario is 5.9, while for NBS2 it is 2.5, a 57% decrease and strong increase in the choking effect. The decreased P is driven by all three changes imposed in NBS2: The 33% change in mean width, the 18% decrease in mean depth and a 56% increase in bed drag coefficient (Mannings-n was increased from 0.020 to 0.025, equivalent to a drag coefficient rise from 0.0021 to 0.0033). Depth enters the choking number as $H^{3/2}$ (Eq. 4) and thus exerts a similar influence on the calculated decrease (-28%) as width *b* (-30%), while drag coefficient enters as $C_D^{1/2}$, diminishing its effect (-21%). A similar influence of inlet depth and width changes is observed in simulations of the historical Jamaica Bay inlet (Orton et al., 2020) and in evaluations of long-term historical changes in other inlet systems such as Biscayne Bay (De Leo et al., 2022). The reduction in choking number P for NBS1 is a much smaller 6.6%, driven exclusively by the 7.1% increase in bay area. Thus, a much smaller decrease in flooding is observed in NBS1.

Table 3: Computed flood dynamics and energetics parameters (with % change from Control)

Scenario	**Choking Number[a] P**	**Bay total[b] Dissipation (PJ)**	**Bay energy increase (PJ)**	**Storm tide prism (km^3)**	**Interior mean bay area (km^2)**	**Box model water rise[c] (m)**	**2D model water rise (m)**
Control	5.75	0.75	10.7	0.168	57.9	2.91	2.93
TSP	n/a	0.12 (-84%)	0.884 (-92%)	n/a	52.6 (-9.2%)	n/a	0.18 (-94%)
NBS1	5.37 (-6.6%)	0.78 (+3.3%)	10.6 (-1.0%)	0.174 (+3.2%)	62.0 (+7.1%)	2.80 (-3.1%)	2.89 (-1.4%)
NBS2	2.36 (-59%)	0.89 (+18%)	6.52 (-39%)	0.124 (-26%)	56.7 (-2.0%)	2.19 (-24%)	2.20 (-25%)

[a] Applying values given in **Table 1** with the Control simulation water rise of 2.82 m
[b] Bay total dissipation includes the inlet
[c] Water rises are bay-wide averages of the rise from low water to peak storm tide

The storm tide prism is substantially reduced by NBS2 (-26%) but increased in NBS1 (+3.2%) (**Table 3**). The NBS2 reduction in prism arises due to partial reflection and/or dissipation of the flood wave (see **Section 3.3**). The NBS1 scenario expanded the floodplain by 7.1% and would be predicted by a simple scaling estimate (**Section 2.5**) to reduce the water rise by ~7% but instead reduces it only by 1.4%. Similarly, the box model that accounts for the changing tidal prism response overpredicts a reduction of 3.1%. Effectively, the slightly lower water level in the interior bay that arises from spreading into a 7.1% larger floodplain leads to a larger pressure gradient and larger inlet flow velocities, and thus a larger volume of water entering the bay (greater tidal prism).

The potential energy increase within the bay from the storm tide's rise from low to high water under the Control scenario is 10.7 PJ and is reduced by 92% for TSP, by 39% for TSP2 and by 1% by NBS1 (**Table 3**). These reductions may arise from either reflection or dissipation of the flood wave (see **Section 3.3**). The temporal maximum dissipation rates over the period of the rising storm tide across Jamaica Bay and vicinity are shown in **Figure 7**, and the spatially and temporally integrated "total dissipation" for the bay/inlet system is given in **Table 3**. Total dissipation during the rising storm tide is modestly enhanced for NBS1 by 3.3% and for NBS2 by 18%, while it is reduced for TSP by 89%. Dissipation is substantially increased relative to the Control scenario in the narrowed pathways through the inlet in NBS2. The slightly greater dissipation in NBS1 (+3.3%) compared to Control is caused by both increased water speeds in the inlet and bay channels (1.6%) and dissipation in the excavated floodplain wetlands (1.7%) at the northern edge of the bay. On the other hand, in the TSP scenario, dissipation is nearly eliminated in the inlet and bay. In NBS2, dissipation increases by 18%, yet energy flux (potential energy increase in the bay) is reduced by 39%. Below, we explore whether wave reflection dynamics might explain these results.

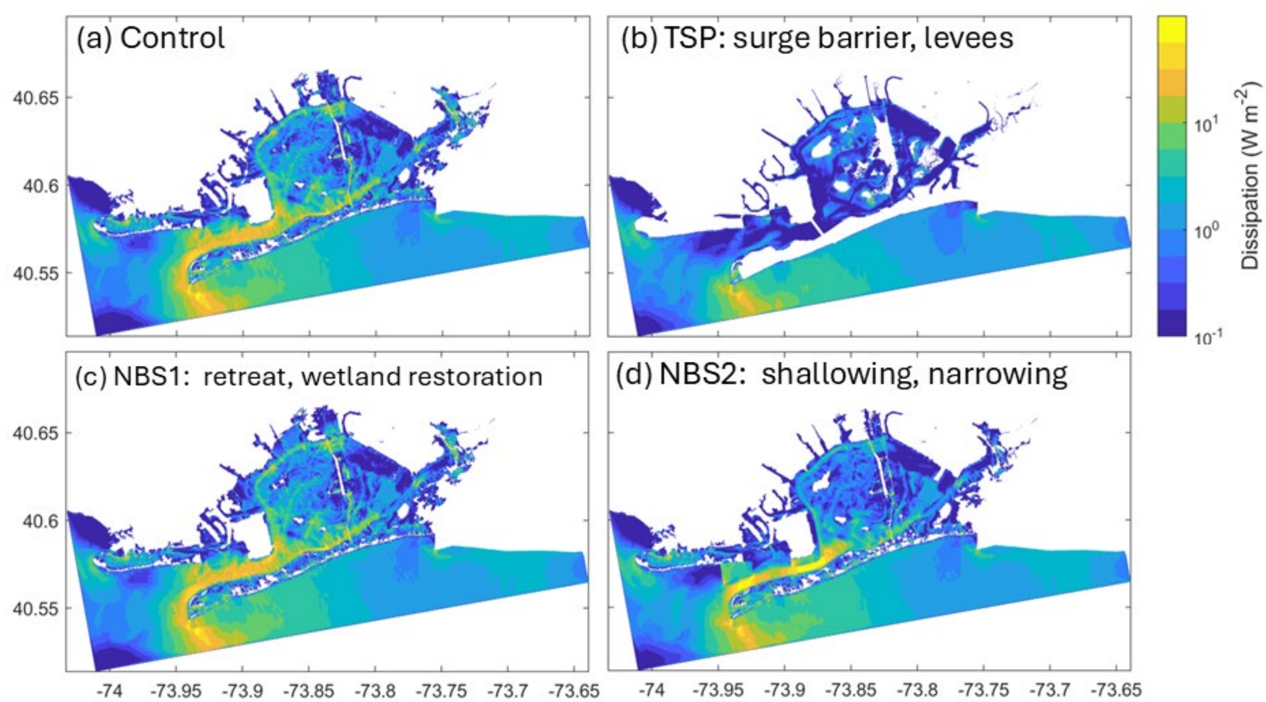

Figure 7: Temporal maximum dissipation rates across the model domain

3.3 Idealized long-wave modelling results

3.3.1 Evaluation of simulated tides

Our idealized model with simplified geometry captures major features of the M2 tide within Jamaica Bay, increasing confidence in its use to evaluate the wave-dynamics of other frequency long-waves (such as storm surge). In the Control scenario, the M2 constituent amplifies by ~14% within the bay (from 0.50 to 0.57 m; **Figure 8a**), similar to the 15% amplification found with the month-long tide simulations on the validated Jamaica Bay 2D model (Pareja-Roman et al., 2023). Decomposing the total M2 wave into incident and reflected components shows that as the incident wave propagates in the landward direction, it gradually attenuates and progresses in phase (**Figure 8c,e**). It fully reflects at the end (20 km) and continues seaward as a reflected wave with nearly the same rate of change in amplitude and phase. Very little difference is observed for the Control scenario between the incident and reflected M2 wave within the bay, indicating minimal dissipation (**Figure 8c**). Further validation for the 1D NBS2 scenario shows damping of the tide by 5% in the bay (**Figure 8a**; relative to Control) qualitatively matches damping of 5-10% seen in the spin-up period of the 2D numerical simulations (**Figure 5**).

However, a few small discrepancies between the idealized 1D modeling and detailed 2D modeling reveal the limitations of its highly idealized landscape and potential inaccuracy near its offshore boundary. The 1D model suggests that a slight 1% amplification in M2 might occur in the back basin of the NBS1 scenario (not found in the 2D modelling). The amplification is likely caused by NBS1 having a larger tidal discharge that partially reflects on the constriction as it exits the basin in a seaward direction. This geometry change between the back basin and constriction in the idealized geometry is larger than that in the detailed 2D model. For TSP, the lower M2 amplitude in the inlet (up to 6 cm lower for km 1-10; **Figure 8a**) is also not visible in the 2D model spin-up periods and is likely an artifact of the requirement of meeting the boundary condition water level at km 0, which is the same restriction across all scenarios. Nevertheless, our application of the idealized model is to gain insight into the long-wave dynamics within the system and the influence of geometric changes, not as a replacement for a detailed numerical model.

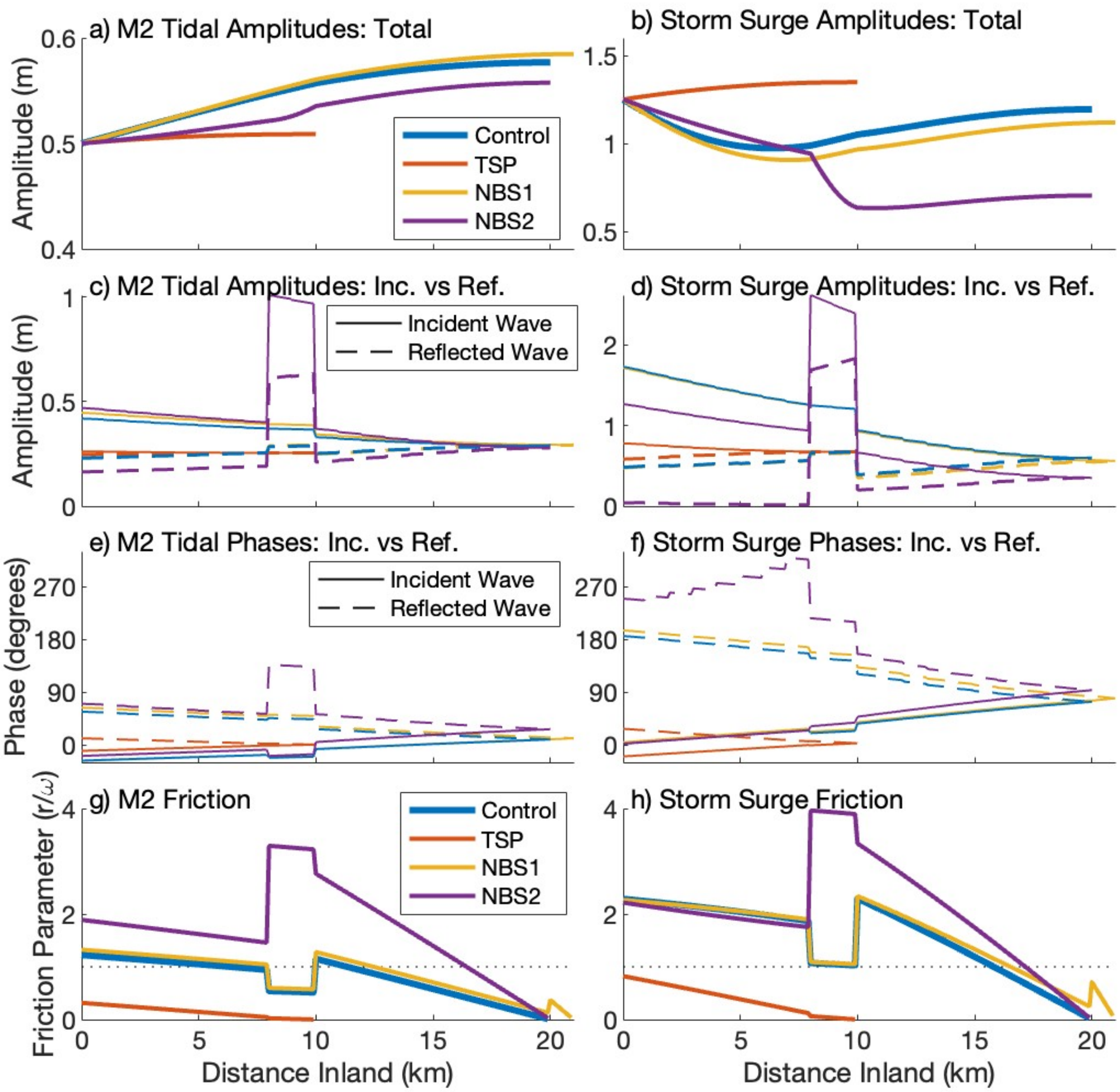

Figure 8: Modeled waves representing M2 tidal waves (left) and the storm surge wave (right), using a 6-hour period surge wave. Modeled geometries are each assigned different colors. Wave amplitudes of the total wave (a, b; thick lines) are decomposed into incident and reflected wave amplitudes (c, d; thin lines) and phases (e, f; thin lines). In panels c to f, line types show the incident (solid) and reflected waves (dashed). The nondimensional friction parameter delineates strongly dissipative r/ω>1 and weakly dissipative r/ω>1 regions (g, h; thick lines).

3.3.2 Tidal reflection characteristics

The M2 dynamics between the four scenarios can be interpreted through consideration of the differences between full and partial reflections. In the TSP scenario, a full reflection occurs at the surge barrier (km 10; **Figure 8c,e**). The nearly overlapping incident and reflected lines show minimal attenuation and a small phase difference is observed. It is important to note that the reflection of the wave is not instantaneous, but occurs over the full wave period, such that in a relatively short basin ($\lambda >> L$), the wave is already interacting with the local geometry as it enters. The contributions through wave interference to the total wave amplitude can be seen in the phase difference between the incident and reflected waves, which approach 0º at the barrier, indicating a maximum positive interference. This full reflection and phase difference is similar to the reflection from the back of the inner basin in the other scenarios where the constructive interference is also strong and causes the total amplitude (**Figure 8a**) to have a similar 'flat' shape with nearly the same amplitudes across the bay. Looking back from inside the bay back into the inlet, as the incident and reflective wave phase difference increases near the mouth, the constructive interference is weaker, and the total amplitude becomes smaller. For a phase difference greater than 90 degrees, as is observed in the inlet's narrowest section (hereafter called the "throat", from km 8-10) for the NBS2 scenario (**Figure 8e**), destructive interference occurs. Thus, any factor which changes the amplitude or phase of the incoming and reflected waves is important for the transmission of the wave signal into the bay.

The spatial changes in phase and amplitude evident in the inlet are driven by abrupt changes in depth and width for all scenarios at km 8 and 10 (**Figure 8**). For the Control and NBS1, the narrowing from the seaward basin to the throat also deepens for almost no change in cross-sectional area (+3%) while the shallowing into the wide bay at km 10 creates a 30% increase in cross-sectional area (**Figure 3**). These changes are much greater for NBS2 with cross-sectional area changes at km 8 and 10 of -66% and +216%, respectively. A width change drives a shift in frictional effects (Eq. 7), through a change in velocity (by continuity). A depth change directly alters the inviscid phase speed $\sqrt{gH}$ (Eq. 6) and the friction parameter, through both velocity and depth changes (Eq. 7). Thus, large shifts in the phase and amplitude of both the incident and the reflected wave are induced at both ends of the inlet section, where width and depth change (e.g., **Figure 8c,e**).

As described also in Dykstra et al. (2024), the reflected wave at any point is the sum of both a total reflection at the boundary (which decays in the seaward direction) and any previous partial reflections in the system (which also decay). For the Control and NBS1 scenarios, their same dimensions in the inlet throat (km 8-10) cause similar small shifts in the incident and reflected waves at the two partial reflection locations (km 8 and 10). The longer NBS1 bay with a larger tidal prism drives small differences (see blue and yellow lines, **Figure 8c,e**). A much more dramatic shift is observed in NBS2. As shown, a partial wave reflection is induced at both ends of the throat, producing a step-function shift in the wave phases (**Figure 8e**). The step function is enhanced by the fully reflected wave, propagating seaward from the back of the estuary, which also reflects at both ends of the inlet. Because the wave solution (Eq. 5) resolves all landward propagating waves as incident and seaward propagating waves as reflected, the interactions become compounded and the exact dynamics of each wave are not explicitly separated. Nonetheless, the energy of near and far field effects are conserved through the inlet with a phase difference causing strong destructive interference and large amplitudes and step changes. Thus, we gain insights into the influence of geometry on the observed wave (**Figure 8a**) through evaluation of the component incident and reflected waves (**Figure 8c,e**).

3.3.3 Storm surge reflection characteristics

The influence of geometry on storm surge is next evaluated by investigating wave mechanics of idealized sinusoidal waves with a similar time scale (period) and amplitude as the simulated storm surge. The idealized surge amplitudes in **Figure 8b** are similar to the numerical results (**Figure 4**), if (a) they are doubled to account for the total rise between low and high water and (b) the predicted tide is added, to convert to total water level. The largest idealized wave amplitudes are observed for TSP. The NBS1 scenario produces a slight decrease in bay-amplitudes, and the most diminished amplitudes are observed for NBS2. The consistency with numerical model results indicates that the simplified model is likely capturing the major dynamics.

Total wave amplitudes during the surge-like wave event (**Figure 8b**) can be interpreted through the lens of full and partial reflections (**Figure 8d,f**). The TSP scenario is the simplest to interpret: the incident wave phase increases in a landward direction while the amplitude slightly decreases until reaching the barrier at 10 km where a full reflection occurs and continues seaward as a reflected wave. Compared to the tide, the shorter surge period causes the phase to progress more from km 0-10 (compare **Figure 8e** and **8f**; TSP scenario). The shorter period and larger amplitude of the "surge" wave increases the velocity and further contributes to more friction. The elevated friction further slows the wave and increases the rate at which the surge attenuates (for more on friction, see **Section 3.3.4** below). The phase difference between the incident and reflected waves increases from near 0º at the barrier to nearly 50º at the mouth, decreasing the positive interference and the total amplitude. For the other scenarios where the strongest reflection was also a full reflection (Control and NBS1 at km 20 or 21), the largest difference in the surge relative to the tide is the larger phase difference between incident and reflected wave. Within the bay, the phase difference exceeds 90º and causes negative interference in most of the model domain to reduce the total wave amplitude.

The Control and NBS scenarios for incident and reflected surge waves all show large changes in amplitude, again revealing significant partial reflections at locations where the geometry changes. The simplest partial reflection occurs at km 20 for NBS1, where the basin ends for the Control and NBS2 scenarios with a full wave reflection. For NBS1, the landward shallow water allows the incident wave to continue (i.e., transmitted wave), dividing energy between the incident and partially reflected waves. The reflected wave's small phase increase of about 10 degrees (**Figure 8f**) helps reduce the total wave amplitude in the bay through being more out-of-phase with the incident wave. A larger partial reflection occurs at km 10 where the basin widens and the incident wave amplitude decreases and the phase increases. At this point, the reflected wave, propagating in a seaward direction, also exhibits a phase increase.

For NBS2, the strong narrowing and shallowing from 8-10 km is resolved for the surge with incident and reflected waves being nearly 180º out of phase, creating stronger negative interference than in the Control and NBS1 scenarios. Even though the incident and reflected wave amplitudes are shown to be the largest (**Figure 8d**), their negative inference (**Figure 8f**) makes this the smallest total amplitude (**Figure 8b**). The narrow constriction for NBS2 of the incoming wave at km 8 creates a partially reflected wave that makes the total amplitude in the seaward region higher than the Control and NBS1 scenarios. The near-zero amplitude of the reflected wave in this region is caused by the nearly 180-degree phase difference between the partially reflected wave originating at km 8 and the fully reflected wave originating at km 20. Overall, the narrowing and shallowing of NBS2 reduce the surge wave amplitude in the bay and through partial reflection, phase shifting, and resulting destructive interference, also cause very little increase in water levels outside the bay.

3.3.4 Wave reflection effects on friction and dissipation

We next use spatial variations in the frictional parameter $\frac{r}{\omega}$ to identify regions of strong and weak dissipation and explore how that varies between different flood mitigation scenarios. Equation 7 indicates weak dissipation when $\frac{r}{\omega} < 1$ and strong dissipation when $\frac{r}{\omega}>1$. In the TSP scenario, $\frac{r}{\omega}$ is weakly dissipative and decreases to 0 at the reflective boundary (km 10), following the steady decrease in velocity that must occur as the discharge becomes 0 at the barrier (**Figure 8g,h**). The other scenarios are also weakly dissipative near their full reflection points in the back barrier, where the overall tidal attenuation is also weak (**Figure 8a,b**). As discharge increases seaward across the back basin, $\frac{r}{\omega}$ increases linearly and at a faster rate for NBS2 (**Figure 8g,h**), driven by the shallower depth and higher drag. Friction similarly increases seaward across the front basin (0-8 km) to the mouth where the largest discharges occur.

The largest difference between scenarios occurs in the inlet throat where Control and NBS1 scenarios show a relatively low $\frac{r}{\omega}$ while NBS2 is relatively high (**Figure 8g,h**). Entering the throat at km 8, Control and NBS1 scenarios become narrower and deeper with nearly no cross-sectional area change, but $\frac{r}{\omega}$ decreases due to depth changes having more influence on friction than area or width. Even though NBS2 also becomes deeper at km 8, the much larger decrease in width reduces the cross-sectional area, causing a constriction that strongly increases velocity and $\frac{r}{\omega}$, supporting choking number calculations. A slightly larger $\frac{r}{\omega}$ in NBS1, relative to Control, is attributed to the longer basin creating a larger tidal prism and stronger currents (**Figure 8g,h**).

The friction parameter $\frac{r}{\omega}$ shows similar patterns for M2 and surge scenarios (**Figure 8g,h**) even though all M2 scenarios amplify landward while most surge scenarios first attenuate before amplifying (**Figure 8a,b**). The relatively smaller M2 wave amplitude has a smaller $\frac{r}{\omega}$ which causes the incident and reflective waves to progress with minimal differences and makes them nearly symmetric in amplitude and phase (**Figure 8c,e**). In contrast, the stronger surge wave $\frac{r}{\omega}$ causes more attenuation and increases asymmetry with the incident waves changing more over a given distance than the reflected waves. These effects are most evident in the NBS2 scenarios where the M2 wave and the surge wave have similar $\frac{r}{\omega}$ in the front basin (0-8 km) as M2 amplifies while the surge attenuates. The high surge $\frac{r}{\omega}$ further landward constricts and slows the wave progression and discharge, subsequently decreasing the tidal prism. Thus, the larger amplitude and shorter period waveform that increases wave discharge and inlet choking effects (Eq. 4), can also reduce the tidal prism and increase dissipation effects on the reflected wave. Furthermore, the results indicate that as dissipation and choking effects increase through geometric effects constricting flow or the waveform growing in amplitude or decreasing in period, the back basin estuary becomes less hydraulicly connected to the sea and will experience relatively less extreme water level changes.

4. Discussion

This research advances our understanding of coastal flood mitigation and induced flooding by evaluating theoretically and numerically the reasons why inlet modification can be a more effective nature-based solution than wetland restoration, while producing a much smaller offshore water level increase than a surge barrier. Dissipation and increased storage are often cited as benefits of nature-based solutions but have only rarely been quantified; assessing mitigation scenarios for Jamaica Bay, we show that much more dissipation often occurs in the inlet than in restored wetlands (due to much larger currents), and that increased storage (allowing the spread of a flood wave) is counteracted, to some extent, by an increase in the total volume of water entering the bay. Most notably, we show that the influence of different adaptation solutions can usefully be interpreted through analysis of the effects of partial and full reflections. For example, nature-based solutions work well if the design enables partially reflected waves to destructively interfere with the incoming waves, hence minimizing induced flooding. Furthermore, our results show how dissipation and reflection can both play an important role in flood wave reductions due to nature-based solutions.

Our approach of using 2D hydrodynamic flood modeling alongside process analysis and idealized modeling can be replicated more widely to quantitatively analyze the mechanisms behind flood mitigation and inducement. The numerous partial reflections exhibited in natural systems make them complex and difficult to understand (and potentially design) when only evaluating water levels. In detailed numerical models, it is often challenging to understand the dynamical reasons for results. The idealized modeling and the concept of partial reflections provide a different, but complimentary, approach for interpreting how specific interventions alter wave propagation.

Below, we further discuss the effects of increasing floodplain storage (**Section 4.1**), increasing dissipation (**Section 4.2**), and altering/inducing a partial flood wave reflection through a change in wave speed (e.g., caused by shallowing of depth, constrictions in width, or altered bed roughness) (**Section 4.3**). Our analyses reveal large differences between the enlisted mechanisms and impacts of nature-based and gray infrastructure mitigation strategies, which can help inform adjustment of these approaches or help develop hybrid approaches that maximize their benefits. Specific design clues are revealed that could help optimize flood mitigation strategies, such as the relative importance of depth, width and frictional changes on flood mitigation and inducement, and the importance of location of tidal marshes within a bay system for flood reduction and inducement (**Section 4.3**).

4.1 Coastal floodwater storage

Our analysis quantifies the degree to which opening up a new floodplain through retreat and excavation of low-lying land can reduce water levels in storm surge scenarios, compared to previously studied evaluations of tidal processes (e.g., Brand et al., 2025; Holleman & Stacey, 2014; Lee et al., 2017; Nederhoff et al., 2025). In river and tidal river systems, allowing a river to spread can reduce peak water levels during a flood wave, particularly if the floodplain enables downstream transport of water, and not just storage (see e.g., Helaire et al., 2019). The strategy of floodwater storage for reducing the amplitude of a flood wave has also been more broadly studied in urban pluvial (e.g., Turner-Gillespie et al., 2003) and fluvial environments (e.g., Wolff & Burges, 1994; Woltemade & Potter, 1994).

The 2D modelling results show how floodplain expansion for a small urban lagoonal estuary like Jamaica Bay have a limited efficacy for flood mitigation elsewhere in the bay. It is intuitive that increasing a floodplain can reduce peak water levels, by spreading the same volume of water over a larger area. However, the reality is more nuanced in coastal lagoons and bays. When the choking number is large (P>>5), increasing bay surface area produces a negligible effect on an incoming wave amplitude through the inlet. Jamaica Bay is transitional between large and small choking numbers, hence sensitive to altered parameters; thus, an increase in area A_e produces a proportional decrease in the choking number (Eq. 4) and might be expected to exert a large influence on water levels. However, we show that an assumption of a response proportional to Area increase neglects the increase in prism that occurs when area is increased. Our 'box model' (Eq. 3) shows that the benefits from increasing floodplain area are substantially reduced (from 7.1 to 1.4%) by an increase in storm tide prism of 3.2%. Equation 3, our idealized scaling that includes the feedback effect of the changing tide prism gives an estimate of a peak water level reduction of 3.1%, compared with the result of 1.4% in the 2D model (**Table 3**). This overestimate likely results from neglecting hypsometry change, which oversimplifies the effect of a floodplain that wets and dries. Nonetheless, our simple theoretical scaling (Eq. 3) helps explain how increases in storm-tide prism counteract the influence of increased area. As a hypothetical bay moves from unchoked to choked (Eq. 4) with increasing area, the role of prism changes may also alter; for P<<5, waves are damped in the inlet, and area changes likely produce negligible effects. Thus, relating the percentage increase in floodplain area to a proportional decrease in flood heights, while appealing, can cause a large overestimation of the flood reduction benefit, as also shown here. Additional research into how prism is altered with choking number and other system properties might help elucidate conditions in which area changes have a differing net effectiveness.

4.2 Flood wave dissipation

As noted in the introduction, tidal marshes are often cited for their ability to "dissipate" storm surge, yet little if any research has directly quantified their influence on energy dissipation for estuary-scale mitigation of long waves. Results for NBS1 demonstrate how both dissipation and reflection can play a role in the mitigation of a flood wave with marshes. The increased dissipation of 1.7% that occurred in the marsh floodplain likely played a role in reducing peak water levels in the bay. The 1D modelling demonstrates how partial reflection and phase shifting (**Figure 8f**) can also play an important role, along with the increased dissipative behavior in the floodplain and bay (**Figure 8h**).

Our results for NBS2 strongly suggest that dissipation and reflection both play an important role in flood wave reductions. Total dissipation was modestly increased by 18% in the bay and inlet, but the reduction in total energy increase by 40% suggests additional processes were also important. Most notably, the strong constriction or choking of the reduced inlet width, depth, and increased roughness leads to strongly increased dissipation in the inlet region, represented with both the 2D model (**Figure 7**) and 1D idealized modelling (**Figure 8e,f**). However, high dissipation in the inlet may also reflect a high propensity for morphologic change, given that erosion and sediment transport respond nonlinearly to rising water speeds similarly to dissipation (Dean & Dalrymple, 2004). Thus, any nature-based or hybrid green-gray solution that leverages strong dissipation will require additional research on morphologic evolution that could occur or on possible engineered approaches that preserve inlet dimensions.

4.3 Long wave partial reflections with phase shifts

The contrast between nature-based and hard infrastructure strategies is sharp for reflection effects and represents a new understanding of the influence of different flood mitigation strategies that has thus far not appeared in the literature. For the surge barrier, complete reflection occurs when the tide and surge hit the barrier, leading to higher peak water levels offshore of the barrier. For the NBS, a series of partial reflections occur in each of the inlet bay systems, particularly with NBS2 at the narrowest point of the inlet. The convergence (depth and width decrease) within the strongly choked inlet causes an amplification in both the incident and reflected wave, as might be expected by conservation of energy (Green's Law; Green, 1839; Jay, 1991). However, the phase shift in the reflection ameliorates the effect of these increased amplitudes on the combined total wave amplitude. Effectively, the influence of friction and energy loss is exhibited in the idealized model through the nondimensional friction, $\frac{r}{\omega}$. For negligible or small $\frac{r}{\omega}$, the wavenumber approaches the inviscid solution, and Green's Law would hold. The combination of the partially reflected wave and the incident wave serves to alter the energy propagation in the system, according to the modified Green's law paradigm with friction suggested by Jay (1991).

Based on the scaling of the wave number (Eq. 6), we can see that depth is more effective at altering long-wave dynamics than width changes. Engineered changes to depth influence the inviscid wave speed and water speed U, in addition to the H term directly; width alteration, by contrast, is only effective at altering U. The drag coefficient is highly variable in natural systems, particularly with complex bedforms (e.g., Branch et al., 2021), and can feasibly be engineered to influence the wave number and therefore long-wave propagation. Finally, and as also verified by the 2D numerical model, the time scale (frequency) of a long wave (i.e., ω) has a first order influence on the wave number, such that short time-scale events are more frictional.

Multiple partial reflections and a full reflection influence the phase difference between the reflected and incoming wave, and hence the degree of constructive interference. Important factors include the phase at the open ocean and potential back-reflection from there ('radiation effects'), the phase and phase shift of the basin near the mouth, the other reflections within a back basin environment, and potentially the most important, the end of the basin itself. Choking the inlet not only alters the amplitude of a transmitted wave, but it also changes the phase of the transmitted wave and can further affect how it interacts with the phases of the other reflections of an inlet-basin system and shift the interference. Thus, more research is needed to best optimize the partial reflection characteristics of an estuary and make it more 'lossy'. This is the inverse of the problem with electrical transmission, in which impedance is matched between different transmission lines, to avoid the loss of energy. To minimize storm surge and flood risk, impedance should be maximized.

The observation that changes to $r = \frac{8}{3\pi}\frac{C_d U}{H}$ produce a change in wave speed, and thus partial reflection, leads to an interesting conundrum: Why does the NBS1 change in Mannings-n from 0.02 to 0.045 (and thus also to C_D), which was applied to the excavated, restored landscape, not cause a substantial partial reflection effect and change in storm surge magnitude? The answer lies within the full wavenumber, $k_f = \frac{\omega}{\sqrt{gH}}\sqrt{-1 + i\frac{r}{\omega}}$. At the end of the bay, velocity — and hence the $\frac{r}{\omega}$ term — is small, and the imaginary contribution to the wave number (and thus the relative influence of frictional to inviscid effects) is correspondingly less than in the inlet, where velocity is large. A similar result was found in our dissipation analysis, which shows a small, relatively unimportant increase in dissipation in the restored wetlands, but much larger dissipation in the inlet. An implication is that a proportional change in drag coefficient will also produce a much larger partial reflection in the inlet, than near the end of the bay. In other words, the location of wetland restoration, frictional changes, or any other intervention strongly influences its effect.

The US Army Corps maintains over 400 inlets in the United States, many of which are much deeper than their historical depths (e.g., De Leo et al., 2022). Some of these inlets likely occupy a similar parameter space as Jamaica Bay and could see improvements in flood hazard through engineered or nature-based elements that are placed in locations that optimize energy dissipation and produce beneficial partial reflections. By understanding the mechanistic relationships between basin geometry and wave dynamics, we demonstrate how NBS can be used to intentionally alter partial wave reflections. These partial reflections are likely implicit features of flood mitigation measures that remain to be fully explained (e.g., Nederhoff et al., 2025). Other types of interventions, not considered here, may influence long-wave amplitudes in estuaries. We also know that in convergent estuaries, the influence of convergence can amplify tidal amplitudes, if the effect is stronger than friction (Jay, 1991), until a condition of critical convergence (Dykstra et al., 2024; Lanzoni & Seminara, 1998). Estuary and basin geometries that amplify tides are also likely to amplify storm surges with similar periods (Dykstra et al., submitted). On the other hand, the presence of side channels can either reduce or amplify tide amplitudes (Alebregtse et al., 2013; Li et al., 2016). At a junction, or when river flow enters a system, additional partial reflections may occur (see e.g., Dronkers, 1964). Thus, using different types of interventions, it may be possible to develop novel approaches to storm tide mitigation (much like resonance in musical instruments, which can be altered by small changes to geometry and air flow).

5. Summary and Conclusions

This research advances our understanding of coastal flood mitigation and potential induced flooding through quantitative analysis and mechanistic interpretation of the effects of flood mitigation strategies. We study a 100-year coastal flood for Jamaica Bay, New York, by applying hydrodynamic modelling for detailed quantification of the effects of flood mitigation and a 1D semi-analytical model in simulations with idealized geometries to further investigate flood reflection processes. We evaluate three flood mitigation scenarios including (a) floodplain and marsh restoration (NBS1), (b) inlet narrowing and bay shallowing (NBS2), and (c) a proposed surge barrier/levee system (TSP).

Results show that the surge barrier system prevents all bay flooding but induces flood-wave reflection and amplification outside the protected area, reducing flooding by 41 km^2. It causes almost no induced flooding due to protection measures along coastlines outside the bay. Of the nature-based solutions, NBS2 provides the largest flood reduction benefit and largest ratio of flood reduction to redistribution, relative to NBS1. NBS2 prevents flooding in 9.5 km^2 and causes only 0.17 km^2 of flood initiation (a 56 times smaller area), in spite of not having shoreline protection outside the bay. This occurs due to both dissipation and partial reflection that causes phase-shifted reflective waves from the inlet throat (km 8-10) and head of bay (km 20) to nearly cancel, minimizing the total water level increase in the inlet and outside the bay. In contrast, NBS1 provides a smaller flood reduction benefit of 0.8 km^2 and 0.07 km^2 of initiation. The lower benefit arises from a feedback process of an increased tidal prism that brings more water into the bay, and due to the partial reflection located at the head of bay that only subtly shifts phase of the reflected wave.

The lasting impact of this research will be to improve our understanding of NBS for mitigating coastal flooding, promoting the development of strategies that go beyond the effective, but inelegant and often unpopular solution of building higher walls against the seas. Nature-based strategies can substantially reduce flooding with minimal flood inducement, and this research reveals the mechanisms by which this can arise. Partial reflection is introduced as a novel mechanism that has not previously been evaluated for flood protection. The clear definitions and quantitative analyses of storage, dissipation and partial reflection, as well as the modeling, demonstrate how these scenarios reduce flooding while minimizing redistribution. These advancements will help optimize the design of NBS and enable their application for their broader range of environmental co-benefits.

Funding sources

PMO was supported by the National Science Foundation (PREEVENTS award no. 1855037) and NOAA (RISA/CAP award NA21OAR4310313). SLD was supported by the Coastal Marine Institute (CMI) and Bureau of Ocean Energy Management (Cooperative Agreement #M24AC00020); and Woolpert, Inc. and the U. S. Joint Airborne Lidar Bathymetry Technical Center of Expertise (JALBTCX). SAT was funded by the Strategic Environmental Research and Development Program (contract W912HQ24C0020).

CRediT authorship contribution statement

Philip M. Orton: Conceptualization, Project Administration, Investigation, Methodology, Validation, Visualization, Writing – original draft, Writing – review and editing. **Steven Dykstra**: Investigation, Methodology, Visualization, Writing – original draft, Writing – review and editing. **Stefan A. Talke**: Investigation, Methodology, Validation, Writing – original draft, Writing – review and editing

Data availability

Data will be made available upon request.

Declaration of competing interests

The authors declare that they have no known competing financial interests or personal relationships that could have appeared to influence the work reported in this paper.

References

Alebregtse, N. C., de Swart, H. E., & Schuttelaars, H. M. (2013). Resonance characteristics of tides in branching channels. *Journal of Fluid Mechanics*, *728*, R3, Article R3. https://doi.org/10.1017/jfm.2013.319

Battjes, J. A., & Labuer, R. J. (2014). *Open Channel flow*. TU Delft.

Blumberg, A., Georgas, N., Yin, L., Herrington, T., & Orton, P. M. (2015). Street scale modeling of storm surge inundation along the New Jersey Hudson River waterfront. *Journal of Atmospheric and Oceanic Technology*. https://doi.org/10.1175/JTECH-D-14-00213.1

Blumberg, A. F., Khan, L. A., & St John, J. (1999). Three-dimensional hydrodynamic model of New York Harbor region. *Journal of Hydraulic Engineering*, *125*(8), 799-816.

Branch, R. A., Horner-Devine, A. R., Chickadel, C. C., Talke, S. A., Clark, D., & Jessup, A. T. (2021). Surface Turbulence Reveals Riverbed Drag Coefficient. *Geophysical Research Letters*, *48*(10), e2020GL092326. https://doi.org/https://doi.org/10.1029/2020GL092326

Brand, M., Diefenderfer, H., Cornu, C., McKeon, M., Janousek, C., Borde, A., Souza, T., Keogh, M., Brown, C., & Bridgham, S. (2025). Can Restoring Tidal Wetlands Reduce Estuarine Nuisance Flooding of Coasts Under Future Sea-Level Rise? *Earth's Future*, *13*(3), e2023EF004149.

Chant, R. J., Ralston, D. K., Ganju, N. K., Pianca, C., Simonson, A. E., & Cartwright, R. A. (2021). Sediment budget estimates for a highly impacted embayment with extensive wetland loss. *Estuaries and Coasts*, *44*, 608-626.

Chernetsky, A. S., Schuttelaars, H. M., & Talke, S. A. (2010). The effect of tidal asymmetry and temporal settling lag on sediment trapping in tidal estuaries. *Ocean Dynamics*, *60*(5), 1219-1241.

De Leo, F., Talke, S. A., Orton, P. M., & Wahl, T. (2022). The effect of harbor developments on future high-tide flooding in Miami, Florida. *Journal of Geophysical Research: Oceans*(Article ID: JGRC25117). https://doi.org/10.1029/2022JC018496

Dean, R. G., & Dalrymple, R. A. (2004). *Coastal processes with engineering applications*. Cambridge University Press.

Dronkers, J. J. (1964). *Tidal Computations in Rivers and Coastal Waters*. North Holland Publishing Company.

Dykstra, S. L., Talke, S. A., Jay, D., Lobo, M., Innocenti, S., & Matte, P. (submitted). Storm Surge and Tides in Convergent Estuaries: the case of Extratropical Storm Merbok in Alaska. *Continental Shelf Research*, *PECS Special Issue*.

Dykstra, S. L., Talke, S. A., Yankovsky, A. E., Torres, R., & Viparelli, E. (2024). Reflection of storm surge and tides in convergent estuaries with dams, the case of Charleston, USA. *Journal of Geophysical Research: Oceans*, *129*(9), e2023JC020498.

Eagleson, P. S., & Dean, R. G. (1966). Small Amplitude Wave Theory. In A. T. Ippen (Ed.), *Estuary and Coastline Hydrodynamics*.

Familkhalili, R., Talke, S., & Jay, D. (2020). Tide-Storm Surge Interactions in Highly Altered Estuaries: How Channel Deepening Increases Surge Vulnerability. *Journal of Geophysical Research: Oceans*, *125*(4), e2019JC015286.

Figueroa, S. M., & Son, M. (2024). Estuarine dams and weirs: Global analysis and synthesis. *Marine Geology*, *477*, 107388. https://doi.org/https://doi.org/10.1016/j.margeo.2024.107388

Fischbach, J., Knopman, D., Smith, H., Orton, P. M., Sanderson, E., Fisher, K., Moray, N., Friedberg, A., & Parris, A. (2018). Building Resilience in a Coastal Environment: Integrated, Science-Based Planning in Jamaica Bay, New York. In (pp. 118): RAND Corporation.

Georgas, N. (2012). Large Seasonal Modulation of Tides due to Ice Cover Friction in a Midlatitude Estuary*. *Journal of Physical Oceanography*, *42*(3), 352-369.

Giese, B., & Jay, D. (1989). Modelling tidal energetics of the Columbia River estuary. *Estuarine, Coastal and Shelf Science*, *29*(6), 549-571.

Gupta, A., Bilskie, M. V., & Woodson, C. B. (2025). The potential of wetlands and barrier islands as a coastal defense in mitigating the storm surge [Original Research]. *Frontiers in Ecology and Evolution*, *Volume 13 - 2025*. https://doi.org/10.3389/fevo.2025.1524570

Hall, T., & Yonekura, E. (2013). North American tropical cyclone landfall and SST: A statistical model study. *Journal of Climate*, *26*(21), 8422-8439.

Helaire, L. T., Talke, S. A., Jay, D. A., & Mahedy, D. (2019). Historical changes in Lower Columbia River and estuary floods: A numerical study. *Journal of Geophysical Research: Oceans*, *124*(11), 7926-7946.

Holleman, R. C., & Stacey, M. T. (2014). Coupling of sea level rise, tidal amplification, and inundation. *Journal of Physical Oceanography*, *44*(5), 1439-1455.

Hu, K., Chen, Q., Wang, H., Hartig, E. K., & Orton, P. M. (2018). Numerical modeling of salt marsh morphological change induced by Hurricane Sandy. *Coastal Engineering*, *132*, 63-81.

Ippen, A. T. (1962). *Estuary and coastline hydrodynamics*. McGraw-Hill. https://books.google.com/books?id=4ZE6twEACAAJ

Jay, D. A. (1991). Green's law revisited: Tidal long-wave propagation in channels with strong topography. *Journal of Geophysical Research: Oceans*, *96*(C11), 20585-20598.

Kalra, T. S., Ganju, N. K., Aretxabaleta, A. L., Carr, J. A., Defne, Z., & Moriarty, J. M. (2021). Modeling marsh dynamics using a 3-D coupled wave-flow-sediment model. *Frontiers in Marine Science*, *8*, 740921.

Keulegan, G. H. (1967). *Tidal flow in entrances: Water-level fluctuations of basins in communication with seas*. Committee on Tidal Hydraulics, Corps of Engineers, US Army.

Kidd, I. M., Davis, J. A., & Fischer, A. (2017). Total exclusion barrages as sea-level rise mitigators: The geomorphological trade-offs for new installations. *Ocean & Coastal Management*, *143*, 122-135. https://doi.org/https://doi.org/10.1016/j.ocecoaman.2016.08.012

Lanzoni, S., & Seminara, G. (1998). On tide propagation in convergent estuaries. *Journal of Geophysical Research: Oceans*, *103*(C13), 30793-30812.

Lee, S. B., Li, M., & Zhang, F. (2017). Impact of sea level rise on tidal range in Chesapeake and Delaware Bays. *Journal of Geophysical Research: Oceans*, *122*(5), 3917-3938.
Li, C., Schuttelaars, H. M., Roos, P. C., Damveld, J. H., Gong, W., & Hulscher, S. J. (2016). Influence of retention basins on tidal dynamics in estuaries: Application to the Ems estuary. *Ocean & Coastal Management*, *134*, 216-225.
Lighthill, M. J., & Lighthill, J. (2001). *Waves in fluids*. Cambridge university press.
MacMahan, J., van de Kreeke, J., Reniers, A., Elgar, S., Raubenheimer, B., Thornton, E., Weltmer, M., Rynne, P., & Brown, J. (2014). Fortnightly tides and subtidal motions in a choked inlet. *Estuarine, Coastal and Shelf Science*, *150*, 325-331.
Marsooli, R., Orton, P. M., Georgas, N., & Blumberg, A. F. (2016). Three-Dimensional Hydrodynamic Modeling of Coastal Flood Mitigation by Wetlands. *Coastal Engineering*, *111*, 83-94.
Mattocks, C., & Forbes, C. (2008). A real-time, event-triggered storm surge forecasting system for the state of North Carolina. *Ocean modelling*, *25*(3), 95-119.
Murty, T. S. (1984). *Storm surges: meteorological ocean tides*.
Nederhoff, K., Saleh, R., Barnard, P. L., & Stacey, M. (2025). Mitigating Flood Risks in Urban Estuaries: Tidal Dynamics, Shoreline Hardening, Nature-Based Solutions, and Floodgates in San Francisco Bay. *Journal of Waterway, Port, Coastal, and Ocean Engineering*, *151*(6), 04025031.
Orton, P. M., Hall, T. M., Talke, S., Blumberg, A. F., Georgas, N., & Vinogradov, S. (2016). A Validated Tropical-Extratropical Flood Hazard Assessment for New York Harbor. *Journal of Geophysical Research*, *121*. https://doi.org/10.1002/ 2016JC011679
Orton, P. M., MacManus, K., Sanderson, E., Mills, J., Giampieri, M., Fisher, K., Yetman, G., Doxsey-Whitfield, E., Wu, Z., Yin, L., Georgas, N., & Blumberg, A. (2016). Project Final Technical Report: Quantifying the Value and Communicating the Protective Services of Nature-Based Flood Mitigation using Flood Risk Assessment. https://philiporton.com/wp-content/uploads/2016/07/coca_technicalreport_draft2p1.pdf
Orton, P. M., Sanderson, E. W., Talke, S. A., Giampieri, M., & MacManus, K. (2020). Storm tide amplification and habitat changes due to urbanization of a lagoonal estuary. *Nat. Hazards Earth Syst. Sci.*, *20*(9), 2415-2432. https://doi.org/10.5194/nhess-20-2415-2020
Orton, P. M., Talke, S. A., Jay, D. A., Yin, L., Blumberg, A. F., Georgas, N., Zhao, H., Roberts, H. J., & MacManus, K. (2015). Channel Shallowing as Mitigation of Coastal Flooding. *Journal of Marine Science and Engineering*, *3*(3), 654-673. https://doi.org/10.3390/jmse3030654
Pareja-Roman, L. F., Orton, P. M., & Talke, S. A. (2023). Effect of Estuary Urbanization on Tidal Dynamics and High Tide Flooding in a Coastal Lagoon. *Journal of Geophysical Research: Oceans*, *128*(1), e2022JC018777. https://doi.org/https://doi.org/10.1029/2022JC018777
Patrick, L., Solecki, W., Gornitz, V., Orton, P. M., & Blumberg, A. (2019). New York City Panel on Climate Change 2019 Report Chapter 5: Mapping Climate Risk. *Annals of the New York Academy of Sciences*, *1439*, 115-125. https://doi.org/10.1111/nyas.14015

Reid, R. O., & Bodine, B. R. (1968). Numerical Model for Storm Surges in Galveston Bay. *Journal of the Waterways and Harbors Division*, *94*(1), 33-57. https://doi.org/doi:10.1061/JWHEAU.0000553

Seavitt, C., Alexander, K., Alessi, D., & Sands, E. (2015). *Shifting Sands: Sedimentary Cycles for Jamaica Bay, New York, in Structures of Coastal Resilience, Phase 1: Context, Site and Vulnerability Analysis*.

Slinger, J. H. (2021). *Building with Nature & Beyond: Principles for designing nature based engineering solutions*. TU Delft OPEN Publishing.

Spicer, P., MacCready, P., & Yang, Z. (2024). Localized Tidal Energy Extraction in Puget Sound Can Adjust Estuary Reflection and Friction, Modifying Barotropic Tides System-Wide. *Journal of Geophysical Research: Oceans*, *129*(5), e2023JC020401. https://doi.org/https://doi.org/10.1029/2023JC020401

Stigebrandt, A. (1980). Some aspects of tidal interaction with fjord constrictions. *Estuarine and Coastal Marine Science*, *11*(2), 151-166.

Szpilka, C., Dresback, K., Kolar, R., Feyen, J., & Wang, J. (2016). Improvements for the Western North Atlantic, Caribbean and Gulf of Mexico ADCIRC Tidal Database (EC2015). *Journal of Marine Science and Engineering*, *4*(4), 72. http://www.mdpi.com/2077-1312/4/4/72

Talke, S. A., Familkhalili, R., & Jay, D. A. (2021). The Influence of Channel Deepening on Tides, River Discharge Effects, and Storm Surge. *Journal of Geophysical Research: Oceans*, *126*(5), e2020JC016328. https://doi.org/https://doi.org/10.1029/2020JC016328

Talke, S. A., Mahedy, A., Jay, D. A., Lau, P., Hilley, C., & Hudson, A. (2020). Sea Level, Tidal, and River Flow Trends in the Lower Columbia River Estuary, 1853–present. *Journal of Geophysical Research: Oceans*, *125*(3), e2019JC015656. https://doi.org/https://doi.org/10.1029/2019JC015656

Turner-Gillespie, D. F., Smith, J. A., & Bates, P. D. (2003). Attenuating reaches and the regional flood response of an urbanizing drainage basin. *Advances in Water Resources*, *26*(6), 673-684. https://doi.org/https://doi.org/10.1016/S0309-1708(03)00017-4

USACE. (2022). *New York-New Jersey Harbor and Tributaries Coastal Storm Risk Management Feasibility Study: Draft Integrated Feasibility Report and Tier 1 Environmental Impact Statement*. New York, NY

USACE. (2025). *Guidance for Induced Flooding, Memorandum for Headquarters and Major Subordinate Commands, Districts, and Field Operating Units,* *https://planning.erdc.dren.mil/toolbox/library/MemosandLetters/Memo_GuidanceInducedFlooding_28July2025.pdf*. Washington, DC

Wamsley, T. V., Cialone, M. A., Smith, J. M., Atkinson, J. H., & Rosati, J. D. (2010). The potential of wetlands in reducing storm surge. *Ocean Engineering*, *37*(1), 59-68.

Wolff, C. G., & Burges, S. J. (1994). An analysis of the influence of river channel properties on flood frequency. *Journal of Hydrology*, *153*(1), 317-337. https://doi.org/https://doi.org/10.1016/0022-1694(94)90197-X

Woltemade, C. J., & Potter, K. W. (1994). A watershed modeling analysis of fluvial geomorphologic influences on flood peak attenuation. *Water Resources Research*, *30*(6), 1933-1942. https://doi.org/https://doi.org/10.1029/94WR00323

Wright, L. D., Coleman, J. M., & Thom, B. G. (1973). Processes of Channel Development in a High-Tide-Range Environment: Cambridge Gulf-Ord River Delta, Western Australia. *The Journal of Geology*, *81*(1), 15-41. https://doi.org/10.1086/627805